UNIVERSIDADE DE SÃO PAULO

INSTITUTO DE FÍSICA
CAIXA POSTAL 66318
05315-970 SÃO PAULO - SP
BRASIL

PUBLICAÇÕES

IFUSP/P-1250

TYPE-II INTERMITTENCY IN THE DRIVEN DOUBLE SCROLL CIRCUIT

M.S. Baptista and **I.L. Caldas**
Instituto de Física, Universidade de São Paulo

Novembro/1996

Type-II intermittency in the driven Double Scroll Circuit

M. S. Baptista, I. L. Caldas
Universidade de São Paulo - Instituto de Física
C. P. 66318, CEP 05315-970 São Paulo, S.P., Brazil

17th November 1996

Abstract

In this work, we show experimental evidences, confirmed by numerical results, from type-II intermittency in the driven Double Scroll Circuit. Numerically, we found a new scaling power law dependence on the critical parameter. This result is a consequence of the first identified global bifurcation scenarium for the T^2 torus breakdown observed in this system: a heteroclinic saddle connection is the nonlinear mechanism responsible for the reinjection of the trajectory around a repellor focus. In fact, in this global scenarium the total laminar phase is the spiraling laminar period (usually considered) plus the time the trajectory spends in the vicinity of the saddle points.

I. INTRODUCTION

The Double Scroll Circuit [1] has been studied for its electronic simplicity and variety of non-linear phenomena. The driven versions of this circuit have been extensivelly investigated by many authors [2], [3], [4], [5] which have found many bifurcation phenomena not observed in the non perturbed circuit. In this work, although the perturbed circuit version is not the same as those used in the previous cited references, we found all phenomena observed in the other driven circuits as Hopf-bifurcation, type-I and chaos-chaos

intermittency, hysteresis, inverse cascades, regularity of periodic windows, quasiperiodicity, devil's staircase structures, crisis, frequency entrainment of chaos, period-adding sequence, and phase-locking. Moreover, in this work, for the first time type-II intermittency was observed in the driven Double Scroll Circuit.

Intermittency is a phenomenum related to the onset of chaotic motion. Intermittent systems behave regularly , the laminar phase, and irregularly, the chaotic burst, alternately. Add to that, the time the system spend in the laminar phase depends on the distance $\epsilon = \mid p - p_c \mid$, where p is a parameter, that in this work can be both the amplitude and the frequency of the driven force, and p_c is the critical parameter for which intermittency comes to sight.

In a classical theoretical work about intermittencies, Pomeau and Manneville identified three possible manners the periodic motion loses its stability [6] . So, depending on the way the eigenvalues of the monodromy matrix cross the unit circle we can have type-I (a real engenvalue, +1), type-II (conjugate complex eigenvalues), and type-III (a real engenvalue, -1). After this pioneer work, other types of intermittencies were found [7].

We give especial attention to the type-II intermittence that show up after a limit cycle loses its stability by a subcritical Hopf bifurcation, what generates an unstable focus in the origin. From a mathematical point of view a periodic motion loses its stability if the conjugate complex eigenvalues of the monodromy matrix cross the unit circle. Pomeau and Manneville conjecture that there must exist a global nonlinear mechanism that reinject the trajectory in the vicinity of the limit cycle. To simulate this nonlinear behaviour, they consider the trajectory was randomly reinjected around the focus. However, they do not specify this global nonlinear bifurcation scenarium.

For the determination of the laminar length for the usual type-II intermittency they supposed a random reinjection distribution in a bi-dimensional disk. If this assumption is correct, the predicted length of the laminar phase should have a scaling law $< n > \propto ln(\frac{1}{\epsilon})$ [6]. However, for numerical simulations, and choosing a random reinjection, they found not a logarithmic scaling law but a power law, $< n > \propto \epsilon^{-}\beta$, with $\beta = -0.5$ [6] like the type-I intermittency [8].

After the work of Pomeau and Manneville, a clear theoretical work about type-II intermittency is provided in Ref. [9], where the authors study a periodically driven third-order nonlinear oscillator. They also find a scaling law for the laminar (spiraling) episodes that fits $< n > \propto \epsilon^{-0.5}$. Furthermore,

they show that this result agrees with the theoretical scaling law obtained assuming a one-dimensional reinjection process. In addition, in this work they argue the possibility of the existence of a homoclinic bifurcation, the global bifurcation scenarium that could explain the reinjection process. However, the existence of a Shil'nikov type homoclinic trajectory [10] can only be proved if the drive is turned off, and the appearance of type-II intermittency in such system is only possible if the driven is turned on. Thus, the reinjection process, responsible for the laminar (spiraling) length, is yet an open question, as also pointed out in reference [11].

The type-II intermittency was experimentally verified to occur in an electronic oscillator [12]. In Ref. [13] there is an inverted version of the type-II intermittency corresponding to a spiraling behaviour assimptoptic to the origin. In Ref. [7] a type-II intermittency coexisting with a type-II intermittency is described. In Ref. [11] a double reinjection channel that directs the trajectory to one of the two focus is presented.

In order to better characterize the type-II intermittency we study how the average length of the laminar episodes (regular behaviour) scale with the distance from the parameter V to the critical parameter V_c. For that we first redefine what we call lamimar phase.

Usually, the laminar phase is considered the spiraling evolution of the trajectory from the time when the reinjection process happens up to the chaotic burst. This spiraling behaviour is caused by the existence of a stable repellor focus.

In the driven Double Scroll Circuit, there is a stable repellor focus inside a stable two-frequency torus. We can only obtain a intermittent regime when this torus is destroyed. Before that happens the two-frequency torus grows in size, leading to the appearance of folds, and a heteroclinic saddle conection among the saddle points [14], which is called a homoclinic countour.

In our case, type-II intermittency is found after the heteroclinic saddle connection is created, which happens after the stable two-frequency torus become unstable by a subcritical Hopf bifurcation. Thus, this global bifurcation scenarium explains how the trajectory is reinjected, from the unstable manifolds of the saddle points to the stable focus. Moreover, in addition to the regular spiraling behaviour there is also a regular saddle permanence identified by the time the system spends in the vicinity of the saddle points. So, in this work, we consider as laminar phase the spiraling length, usually treated as the laminar phase of the type-II intermittency, plus the saddle

permanence.

We have also found evidences that the global bifurcation scenarium (the heteroclinic saddle connection) has a tipically homoclinic trajectory to the saddle points.

This paper is organized as follows. In Sec. II we present the driven Double Scroll Circuit and the system of equations that simulates its dynamic. In Sec. III we show experimental observations of the type-II intermittency in this electronic circuit. For a better understanding of the experimental results we show in Sec. IV numerical results confirming the existence of the type-II intermittency transition to chaos. In this section we also show, by analising the Lyapunov exponent, that the onset of chaos in this case is abrupt. Finally, in Sec. V we study the laminar phase length as a function of ϵ. Conclusions are given in Sec. VI.

II. The driven Double Scroll Circuit

This circuit is schematically shown in Fig. 1. It is composed by two capacitors, C_1 and C_2, two resistors, R and r, one inductor, L, and the non-linear resistor, R_{NL}.

The electronic value components used in our experiment are

$$C_1 = 0.0052\ \mu F,\ \ C_2 = 0.056\ \mu F,\ \ R = 1470\ \Omega,\ \ L = 9.2\ mH,\ \ r = 10\ \Omega \quad (1)$$

and the driven force applied to the circuit can be represented by

$$q(t) = V \sin(2\pi f t) \quad (2)$$

where V is the amplitude and f is the frequency. The R_{NL} characteristic curve can be seen in Fig. 2 and is mathematically represented by

$$i_{NR}(V_{c1}) = m_0 V_{c1} + 0.5(m_1 - m_0) \mid V_{c1} + B_p \mid + 0.5(m_0 - m_1) \mid V_{c1} - B_p \mid \quad (3)$$

We can simulate the circuit of Fig. 1 by applying Kirchoff's laws. So, the resulting state equations are

$$C_1\frac{\partial V_{C1}}{\partial t} = \frac{1}{R}(V_{C2} - V_{C1}) - i_{NR}(V_{c1})$$
$$C_2\frac{\partial V_{C2}}{\partial t} = \frac{1}{R}(V_{C1} - V_{C2}) + i_L \qquad (4)$$
$$L\frac{\partial i_L}{\partial t} = -V_{C2} - q(t)$$

where V_{C1} and V_{C2} are the voltage across the capacitors C_1 and C_2, respectively, and i_L is the electric current across the inductor L. To avoid numerical problems we do not use the real component values in Eqs. (4), but we use a rescaled set of parameters given in terms of the real values. Thus, the parameters used in Eqs. (4) for doing numerical simulation of the circuit in Fig. 1 are

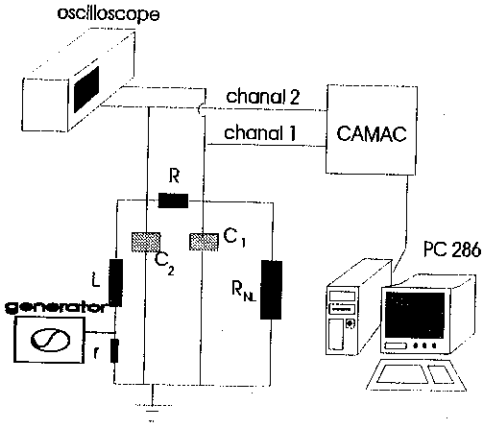

Figure 1: The sinoidally perturbed Double Scroll circuit and the aparatus for the data aquisition.

$$\frac{1}{C_1} = 10.0, \quad \frac{1}{C_2} = 1.0, \quad \frac{1}{L} = 6.0$$
$$\frac{1}{R} = 0.6, \quad m_0 = -0.5, \quad m_1 = -0.8, \quad B_p = 1.0. \qquad (5)$$

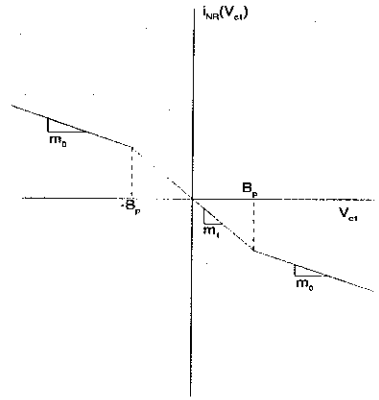

Figure 2: The characteristic curve of the non-linear resistor R_{NL}.

For the electronic components in Eq. (1), or the parameter simulation values in Eq. (5), and for a null perturbing amplitude $V = 0$, the circuit behaves chaotically. As the circuit is dissipative its dynamic variables (V_{C1}, V_{C2}, and i_L) evolve on a chaotic attractor named Double Scroll.

III. The experimental two-frequency torus breakdown

When the driven force is turned on, that means $V \neq 0$, a new frequency is introduced in the characteristic oscillations of the Double Scroll Circuit. This new frequency is responsible for the appearence of a quasi-periodic moviment on a two-frequency torus (T^2).

In Fig. 3, the oscillations in (A) correspond to a limit cycle just after a Hopf bifurcation. In (B) we identify a second Hopf bifurcation of this limit cycle creating a torus T^2. Increasing further the driven frequency, we show in (C) a two-frequency torus breaking through type-II intermittency as confirmed by numerical simulations.

The bi-dimensional projection of the Double Scroll attractor on the plane ($V_{C1} \times V_{C2}$) for the parameters of Figs. 3B and 3C is shown in Fig. 4. In this

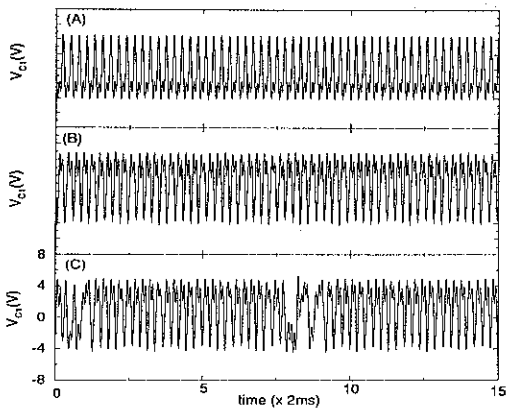

Figure 3: Time evolution of the variable V_{C1} for a fixed amplitude $V = 0.700$ V and frequencies $f = 1.852$ kHz (A), $f = 1.923$ kHz (B) and $f \gtrapprox 1.923$ kHz (C).

figure we see the torus T^2 (A) and its breakdown (B). After the breakdown the attractor grows in size and its trajectory evolves erraticaly all over this plane. This behaviour is only observed in a two-frequency torus breakdown through the type-II intermitency.

To obtain the image of the torus T^2 one must analyze the crossings of the three-dimensional trajectory of the dynamic variables on a Poincaré section. However, as indicated in Fig. 1, we can only collect data from two channels. Therefore, only two dynamical variables are considered, $V_{C1}(t)$ and $V_{C2}(t)$. To obtain the three-dimensional attactor needed to visualize the torus T^2, we reconstruct the 3-D chaotic attractor by using the time-delay method [15].

The considered dynamic variable is $V_{C1}(t)$ and the time-delay (time shift) rate is $p = 24\ \mu s$ (with the aquisition time $\delta = 2\ \mu s$). Thus, for a time series $V_{C1}(t)$, we construct a three dimensional trajectory. The first point of this trajectory is ($V_{C1}(t)$, $V_{C1}(t + p)$, $V_{C1}\ (t + 2p)$), the second is ($V_{C1}\ (t + \delta)$, $V_{C1}\ (t + \delta + p)$, $V_{C1}\ (t + \delta + 2p)$), and so on. In this notation, the reconstructed trajectory has three coordinates represented by (X,Y,Z). Thus, the intersection of a reconstructed torus T^2 with the section X=0 is shown in Fig. 5A. The way chaos appears by torus breakdown is shown in Fig. 5B. In this last figure, the characteristic chaotic bursts due to trajectory

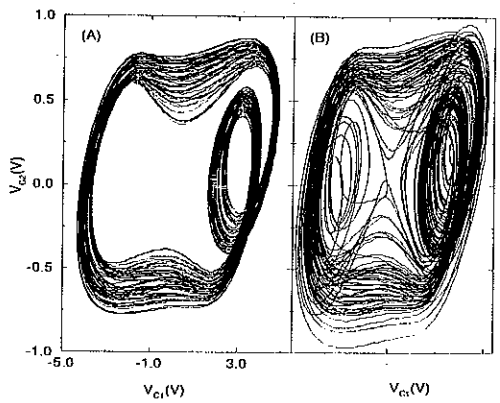

Figure 4: Projection of the attractor on the variable space plane ($V_{C1} \times V_{C2}$) for $f = 1.923$ kHz (A), and $f \gtrapprox 1.923$ kHz (B).

ejections (as analyzed in Sec. IV) can be already identified.

IV. The simulated two-frequency torus breakdown

The route to chaos via torus breakdown, described in Sec. III, is better understood through the numerical results obtained by integrating Eqs. (4) with the parameters given by (5), for a fixed driven frequency $f = 0.18$. Thus, Fig. 6A shows a bifurcation diagram of the variable V_{C2}, when the trajectory crosses a Poincaré section at V_{C1} = -1.5, as a function of V. The abrupt appearance of chaos, seen in this figure, is confirmed by the first Lyapunov exponent λ (Fig. 6B). We have numerically determined that chaos first appears for $V = 0.2328691$ leading to $\lambda > 0$.

In Fig. 7 we see a sequency of three figures showing the attractor through the Poincaré section positioned at V_{C1} = -1.5. So, in this figure we see the attractor through the variables V_{C2} and i_L.

The torus T^2 is created after a supercritical Hopf bifurcation. In this situation, before the onset of chaos, the torus is a deformed circle with no

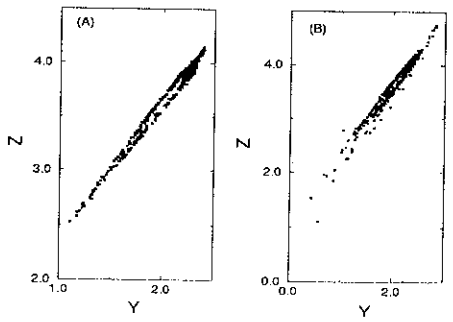

Figure 5: (A) Poincaré section of the reconstructed quasi-periodic torus T^2 of the three dimensional attractor obtained for $V = 0.700$ V and $f = 1.923$ kHz. (B) The torus T^2 breaks generating chaotic behaviour for $V = 0.700$ V and $f \gtrapprox 1.923$ kHz. (A) and (B) have different axis scalings.

folds or cuspides, as shown in Fig. 7A (V= 0.2280000). However, rising the amplitude (V = 0.2328690), the torus T^2 folds in five parts resembling a five-sided polygon (Fig. 7B). The torus breaks as in Fig. 7C (V= 0.2328691) leading to the appearance of type-II intermittency, that causes the trajectory to evolve spirally around the previously existing repellor focus point, indicated in figure by o. So, we can say that the critical parameter is V_c = 0.2328690.

Along the torus, not yet destroyed, a quasi-periodic trajectory is non-clockwise oriented with a winding number near to the racional fraction $w = \frac{3}{5}$. Three is the number of the trajectory rotations along the torus to return back to the same point, taking five complete cycles. It means that, after passing nearby a saddle point of Fig. 7, the trajectory crosses this Poincaré section five times before returning to the same saddle point. We can consider the flow on this section as a mapping G. So if c_n with $n = 1, \ldots, 5$, are the saddle points, then $G^5(c_n) = c_n$ and $G(c_n) = c_{n+1}$.

As a matter of fact, the laminar spiral trajectory is a five-spiral trajectory, which means that the trajectory visits each time one of the five spirals. These spirals evolve approaching asymptotically the previous stable five-sided polygon torus. In fact, each spiral tends to one of the five corners of the polygon.

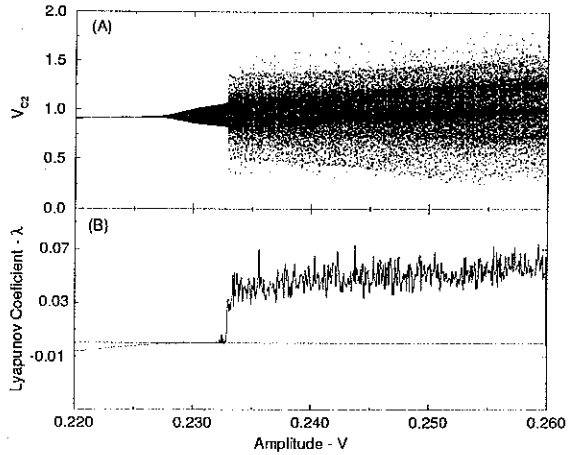

Figure 6: (A) A bifurcation diagram showing the two-frequency torus creation (via Hopf bifurcation) and then its destruction, generating chaotic behaviour, by a rising amplitude V and a fixed driven frequency $f = 0.18$. (B) The first Lyapunov exponent λ, for the same parameters of (A). That means chaos for $\lambda > 0$. $V_{C1} = -1.5$.

These corners , indicated by c_n, are saddle points with two different unstable manifolds. Along one unstable manifold the trajectory is ejected outside the polygon causing the chaotic burst. Along the other the trajectory is directed to the nearest saddle point in the non-clockwise direction (sampling each five steps in the Poincaré section). That means that $G.G^5(c_n)$ tends to c_{n+1}.

In Fig. 7C the unstable manifolds responsible for the chaotic burst are indicated by W_u^1, and those responsible for the heteroclinic saddle connection (an orbit in G^5 that connects the five saddle points) by W_u^2. So, we see that the unstable manifold of the saddle point c_1, $W_u^2(c_1)$ is the stable manifold of the c_3, $W_s^2(c_3)$. This heteroclinic looping is also called a Poincaré homoclinic contour [10].

We will not go into details about the chaotic burst. It is enough, for now, to say that the trajectory approachs the saddle points spiraling, is expelled from the broken torus along W_u^1, and then is reinjected back inside the broken torus (into the focus) leading again to the spiral laminar phase.

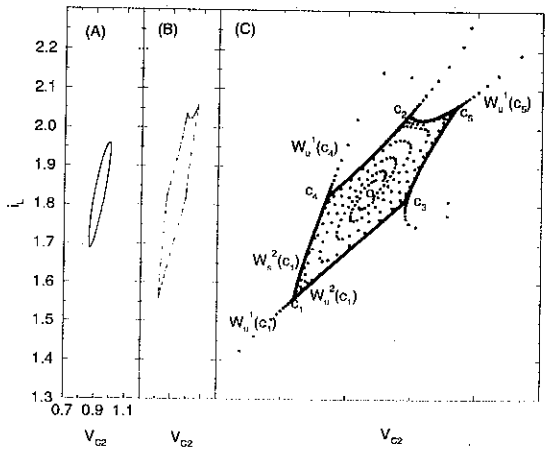

Figure 7: (A) A quasi-periodic torus T^2 for V=0.2300000. (B) The five-sided quasi-periodic folded torus for the critical parameter V=0.2328690. (C) The destruction of the torus leading to a type-II intermittency. $V_{C1} = -1.5$

V. Analysis of the laminar length

As mentioned before, the trajectory stays for a while in the saddle points before it is ejected out of the broken torus. Contrary to what is usually done (when the laminar phase is considered to be the spiraling behaviour), we consider as laminar phase any regular behaviour. So, the laminar phase is due to the spiraling behaviour caused by the repellor focus located at the origin plus the permanency of the trajectory in the vicinity of the saddle points.

In Fig. 8, we show the evolution of the variable V_{C2}^n through the Poincaré section $V_{C1} = 1.5$, where the index n represents the n-th time the trajectory crosses this section. In this figure we see typical spiraling laminar phases and permanency in the saddle points, followed by chaotic bursts, with the trajectory ejected along the unstable manifold of the saddle points.

In figure 8, we see that the permanency in the saddle point is smaller than the spiraling behaviour. In fact, the bigger ϵ the shorter the saddle

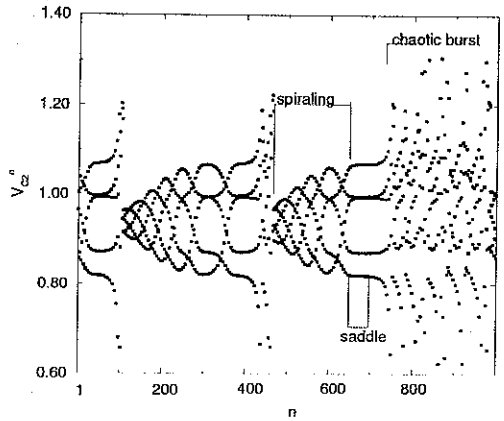

Figure 8: Evolution of the variable V_{C2} through the section V_{C1} = -1.5 showing the laminar length composed by the spiraling behaviour plus the permanency in the saddle point.

permanency. However, for an amplitude very close to the critical value the spiraling length is short. Furthermore, for a rising amplitude, both the spiraling length and the saddle permanency became smaller. In fact, the laminar phase is very complex if we consider it composed by the spiraling behaviour plus the saddle permanence. As we shall see, there is a competition behaviour between these two regular phases.

For numerical analysis, we consider that a point in the Poincaré section represents a laminar trajectory if it is positioned within a polygon composed by the junction of the five saddle points (ploted with a filled circle in Fig. 9) or within the five circunferences of radius ρ =0.005 centered in the saddle points. Naturally, the saddle permanence (S_P) is the number of steps the trajectory spends inside these circunferences. Therefore, if we call the length of the laminar phase as L_P, and the spiraling length as S_L,

$$S_L = L_P - S_P \tag{6}$$

Pomeau and Maneville [6] considered a randomly and spatial uniform

reinjection in the repellor focus to derive their logarithmic scaling law for the laminar (spiraling) phase. Richetti [9] obtained a power scaling law for the laminar (spiraling) behaviour for a unidimensional spatial reinjection. In the driven Double Scroll Circuit we find that the reinjection process due to the heteroclinic saddle connection puts the trajectory in any part near the two-dimensional focus. However, the reinjection placement is not uniform as we can see in Fig. 9, where the squares indicating the first iterations around the focus (the reentrance location) are mainly distributed along two main directions.

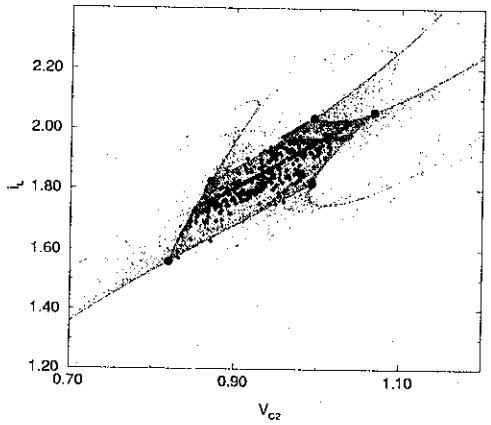

Figure 9: The destructed torus obtained for $f = 0.18$ and $V = 0.2328750$, where we can identify the first points to reenter the focus (filled squares), and the saddle points (filled circles). $V_{C1} = -1.5$, and the number of steps n=200000.

The reentrance distribution along two main directions cause the two-peaks observed in the laminar phase distribution $P(n)$ (where n is the number of times the trajectory crosses the Poincaré section during the laminar behaviour). Each peak decays exponentially $P(n) \propto exp(-2\epsilon n)$ as determined by Pomeau and Manneville [6]. There is one main peak for small n that represents the trajectories reinjected in the neighbourhood of the saddle points and therefore quickly ejected. This is an evidence that there may

exist a homoclinic trajectory through a saddle point, since the trajectory is biasymtoptic to the basic cycle responsible for the saddle points, as we see on the Poincaré section [16].

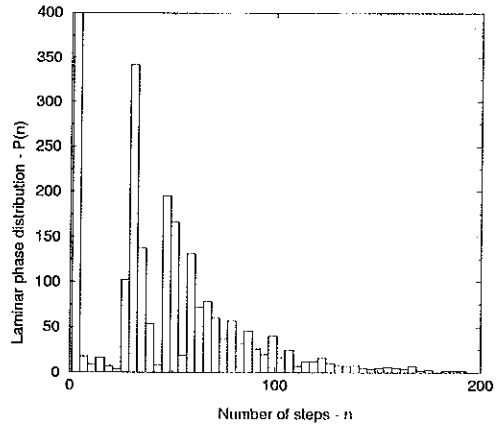

Figure 10: Probability distribution $P(n)$ for the laminar length (the spiralling length plus the saddle permancence). The number of steps n=200000. For the main peak $P(n) \approx 7000$.

We now show a new scaling law for the laminar phase considering the two regular phases: S_L and S_P. Thus, Fig. 11 shows the saddle permanence, S_P, and the laminar phase, L_P, indicated respectively by squares and circles, as a function of ϵ. We fitted this points, and obtained that $S_P \propto \epsilon^{\alpha}$, with $\alpha = -0.542 \pm 0.019$ (the fitted function is indicated by (1)). The laminar phase behaves as $L_P = \frac{1}{A+\beta\epsilon}$, with $\beta = 0.075 \pm 0.002$ and $A = 6 \times 10^{-5}$, for $\epsilon \geq 0.000011$ (indicated by (2)), and $L_P \propto \epsilon^{\gamma}$, with γ = -0.151$\pm$ 0.009, for $\epsilon < 0.000011$ (indicated by (3)).

Using Eq. (6), we can obtain a spiraling length that is distinct from the laminar (spiraling) length predicted by Pomeau and Manneville. Thus, through the fitted functions, S_P and L_P, the spiraling average length, S_L, as a function of ϵ is shown in Fig. 12.

So, the function S_L has a fast growth for $\epsilon < 0.000011$, because $\alpha > \gamma$, and a inverse decay for $\epsilon \geq 0.000011$ because ϵ^{α} vanishes for $\epsilon \geq 0.000011$.

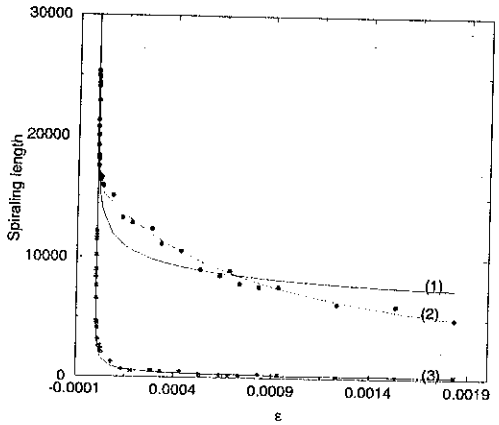

Figure 11: The saddle permanence (square) and the laminar phase (circle) in respect to ϵ. The number of steps n=30000.

This is exactly what we can see in Fig. 12, where the function S_L is shown.

One can say that the fast growth of the spiralling length for $\epsilon < 0.000011$ is a negligible effect because it is localized in a very small neigbourhood of the critical parameter; however, this effect is due to the heteroclinic saddle connection and if we disconsider it, we have to disregard the global bifurcation analisis that sustain the reinjection process.

For $\epsilon > 0.2340000$ there is a saddle disconnection bifurcation [14] and the spiraling behaviour loses its original shape. Before the saddle disconnection, each of the five spirals would go spirally, around the origin, approaching the saddle points. After the saddle disconnection, this spiraling behaviour becomes oriented and a point falling down in the previous stable focus is directed to the saddle point, without present the spiraling behaviour.

The power scaling law for the saddle permanence (with $\alpha = -0.542$) may give us the wrong impression that this permanence would be due to a type-I intermittence. However, the saddle permancence can not be associated to such a phenomenum since, as pointed out in Ref. [16], as a consequence of the marginality of the basic cycle in the intermittent systems, the trajectories

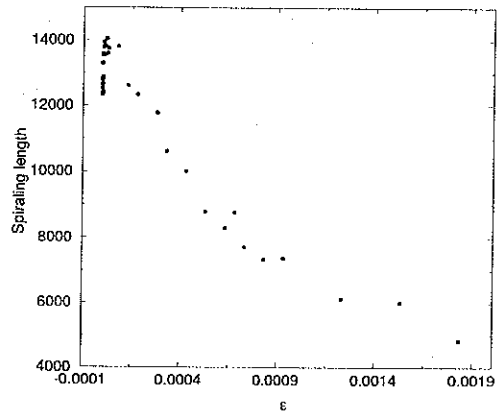

Figure 12: The function S_P, obtained through Eq. (6). The number of steps n=30000.

leaves the cycle as $\frac{1}{t^\mu}$ for $t \to -\infty$ (with $\mu = 1$ for type I intermittency) while the escape from the cycle in systems with a homoclinic tangency behaves like $e^{\alpha t}$ for $t \to -\infty$ (with $\alpha > 0$).

What we found in the neighbourhood of the saddle points is that the trajectory is ejected from these points exponentially as we can see in Fig. 13. In this figure we choose the saddle point c_2 in Fig. 7 and consider a trajectory passing through a neighbourhood δ of this saddle point. After the trajectory crosses the Poincaré section $V_{C1} = -1.5$ at the point $P = (V_{C2}, i_L)$, we analise how δ grows up after n steps. So, for $n = 1$ we see the spatial displacement $\delta = G^5(P) - c_2$, and for $n = 2$ we see $\delta = G^5.G^5(P) - c_2$, and so on.

This result assures that the trajectory leaves the unstable manifold $W_u^2(c_2)$ with an exponentially spatial divergence. Furthermore, the unstable manifold W_u^1 has also an exponential divergence. We know that the junction of the manifolds W_u^2 form the heteroclinic saddle connection (a Poincaré homoclinic contour). Following the same thought, it is natural to believe that from the unstable manifolds W_u^1 there may exist an orbit that leaves the basic cycle along $W_u^1(c_n)$ and returns to this cycle through the stable manifold $W_s(c_m)$

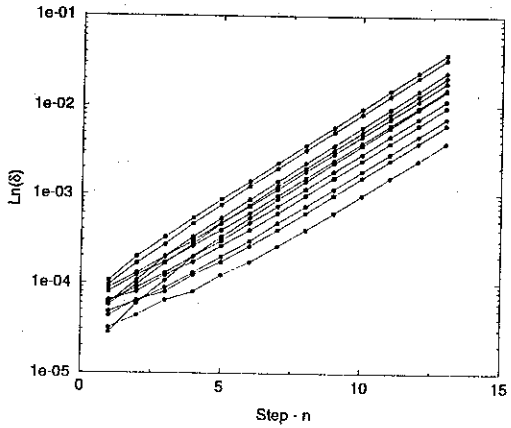

Figure 13: The spacial relative distance δ between a sequence of points P of an ejected trajectory (in the neighbourhood of the point c_2) and the saddle point c_2.

(note that $n \neq m$). If such orbit exists, it is an orbit that is byasimptotic to a saddle point for $t \to \infty$ along the $W_s^2(c_m)$, and for $t \to -\infty$ along the $W_u^1(c_n)$.

In the neighbourhood of such an orbit there exists the Smale Horseshoe process [14], and therefore chaotic motion. That means that its neigbouhood belongs to the vicinity of the repellor focus.

We numerically found at least two orbits that seems to behave like a homoclinic orbit and are localized in the two extremes inside the basic cycle, and, due to their existence, the area inside the atractor of Fig. 4 is filled by trajectories.

The possible existence of this two main homoclinic orbits could explain why we have found two main regions where the reinjection in the focus happens.

VI. Conclusions

In this work we identify, for the driven Double Scroll Circuit, the first global non-linear mechanism responsible for trajectory reinjections around a repellor focus, leading to the type II intermittency. This mechanism is a heteroclinic saddle connection that surrounds the repellor focus. Because of such a scenarium, the considered laminar phase is the time the trajectory spends in the vicinity of the saddle points plus the spiraling length around the focus.

We have found that this new considered laminar phase, L_P, scales as $L_P \propto \epsilon^{\gamma}$, with γ = -0.151± 0.009, for $\epsilon < 0.000011$, and $L_P = \frac{1}{A+\beta\epsilon}$, with $\beta = 0.075 \pm 0.002$ and $A = 6 \times 10^{-5}$, for $\epsilon \geq 0.000011$.

Although the trajectory reinjection is typically two-dimensional, the set of reentry points is mainly distributed along two directions. This reentrance causes the appearance of two peaks in the probability distribution for the laminar length. Each peak decays exponentially $P(n) \propto exp(-2\epsilon n)$, as predicted by Pomeau and Manneville for a reentrance model with a random uniform two-dimensional distribution. Besides these two peaks there is one main peak that represents a trajectory reinjected along the stable manifold of a saddle point and quickly expelled along the unstable manifold. Th existence of this peak is a strong evidence of the presence of a homoclinic trajectory to the heteroclinic saddle connection.

The saddle permanence may be erronealy interpreted as the regular phase of a type-I intermittency because of its observed scaling power law. However, we have shown that the spatial escape along the unstable manifold of the saddle points is exponential, typical of homoclinic tangencies, one more evidence about the existence of a homoclinic trajectory to the saddle points.

Finally, we have numerically found two orbits that seems to behave as a homoclinic orbit to the saddle points. If such orbits exist in its neighbourhood there is an Smalle Horseshoe process that would be the reason for the reinjection process. Naturally, the neighbourhood of this orbit belongs to the vicinity of the repellor focus and so the reinjection process is explained.

Acknowledgments

The authors thank Mr. A. P. Reis for the assistance in the electronic aparatus, Dr. A. N. Fagundes for making the codes for the data aquisition, and

for useful computation advices, the computacional assistance of Dr. W. P. de Sá, and Dr. J. C. Sartorelli for its useful experimental advices and the assistance in the experimental work. We also thank Herr K. Ullmann for his useful suggestions. This work was partially supported by FAPESP and CNPq.

References

[1] T. Matsumoto and L. O. Chua, IEEE Trans. Circuits Syst. **CAS-32**, 797 (1985).

[2] M. Itoh, H. Murakami, and L. O. Chua, Int. J. Bifurcation and Chaos **4**, 1721 (1994).

[3] K. Murali and M. Lakshmanan, Int. J. Bifurcation and Chaos **2**, 621 (1992).

[4] L. Pivka, A. L. Zheleznyak, and L. O. Chua, Int. J. Bifurcation and Chaos **4**, 1743 (1994).

[5] K. Murali and M. Lakshmanan, Int. J. Bifurcation and Chaos **1**, 369 (1991).

[6] Y. Pomeau and Paul Manneville, Phys. Lett. A **79**, 33 (1980); Commun. Math. Phys. **74**, 189 (1980).

[7] G. J. de Valcárcel, E. Roldán, Víctor Espinosa and R. Vilaseca, Phys. Lett. A **206**, 359 (1995).

[8] M. S. Baptista and I. L. Caldas, Chaos, Solitons, and Fractals **7**, 325 (1996).

[9] P. Richetti, F. Argoul, and A. Arneodo, Phys. Rev. A **34**, 726 (1986).

[10] L. P. Shil'nikov, Int. J. Bifurcation and Chaos **4**, 489 (1994).

[11] J. San-Martín and J. C. Antoranz, Phys. Lett. A **219**, 69 (1996).

[12] J.-Y. Huang and J.-J. Kim, Phys. Rev. A **36**, 1495 (1987).

[13] J. Sacher, W. Elsässer and E. O. Göbel, Phys. Rev. Lett. **63**, 2224 (1989).

[14] D. K. Arrowsmith and C. M. Place, *An Introduction to Dynamical Systems*, Cambridge University Press, UK, 1990.

[15] F. Takens, *Dynamical Systems and Turbulence*, Springer-Verlag, Berlin, GR, 1980.

[16] P. Gaspar and X.-J. Wang, J. Stat. Phys. **48**, 151 (1987).